

1 *Trypanosoma brucei* colonises the tsetse gut via an immature  
2 peritrophic matrix in the proventriculus

3

4 Clair Rose<sup>1,2,‡\*</sup>, Naomi A. Dyer<sup>1,2,‡</sup>, Aitor Casas-Sanchez<sup>1,2,‡</sup>, Alison J. Beckett<sup>3</sup>, Carla  
5 Solórzano<sup>2,†</sup>, Ben Middlehurst<sup>3</sup>, Marco Marcello<sup>4</sup>, Michael J. Lehane<sup>1</sup>, Ian A. Prior<sup>3,5</sup> and Álvaro  
6 Acosta-Serrano<sup>1,2,\*</sup>

7

8 <sup>1</sup>Department of Vector Biology and <sup>2</sup>Department of Parasitology, Liverpool School of Tropical  
9 Medicine, Liverpool, UK. <sup>3</sup>EM Unit, Department of Cellular and Molecular Physiology, Institute  
10 of Translational Medicine, University of Liverpool, Liverpool, UK. <sup>4</sup>Centre for Cell Imaging,  
11 Institute of Integrative Biology, University of Liverpool, Liverpool, UK. <sup>5</sup>Physiological  
12 Laboratory, Institute of Translational Medicine, University of Liverpool, Liverpool, UK.

13

14 ‡These authors contributed equally.

15 †Present address: Department of Clinical Sciences, Liverpool School of Tropical Medicine,  
16 England, UK.

17

18 \*Co-corresponding authors. e-mail: [Clair.rose@lstmed.ac.uk](mailto:Clair.rose@lstmed.ac.uk) and [alvaro.acosta-  
19 serrano@lstmed.ac.uk](mailto:alvaro.acosta-serrano@lstmed.ac.uk)

20

21 Contact during submission: [alvaro.acosta-serrano@lstmed.ac.uk](mailto:alvaro.acosta-serrano@lstmed.ac.uk)

22

23 Note: Supplementary videos are not included in this version

24

25

26 **Abstract**

27 The peritrophic matrix (PM) of haematophagous insects is a chitinous structure that surrounds  
28 the bloodmeal, forming a protective barrier against oral pathogens and abrasive particles. To  
29 establish an infection in the tsetse midgut, *Trypanosoma brucei* must colonise the  
30 ectoperitrophic space (ES), located between the PM and gut epithelium. Although unproven,  
31 it is generally accepted that trypanosomes reach the ES by directly penetrating the PM in the  
32 anterior midgut. Here we revisited this event by employing novel fluorescence and electron  
33 microscopy methodologies and found that instead, trypanosomes reach the ES via the newly  
34 secreted PM in the tsetse proventriculus. Within this model, parasites colonising the  
35 proventriculus can either migrate to the ES or become trapped within PM layers forming cysts  
36 that move along the entire gut as the PM gets remodelled. Early proventricular colonisation  
37 appears to be promoted by unidentified factors in trypanosome-infected blood, resulting in  
38 higher salivary gland infections and potentially increasing parasite transmission.

39

40

41

42

43

44

45

46

47

48

49

## 50 Introduction

51 *Trypanosoma brucei* sub-species, the causative agent of human sleeping sickness and also  
52 partially responsible for animal trypanosomiasis in sub-Saharan Africa, are transmitted  
53 exclusively by flies of the family Glossinidae, commonly known as tsetse. These parasites  
54 have a complex life cycle within the fly, but key to transmission is the ability to first establish  
55 an infection within the insect midgut. After a fly ingests blood from an infected mammal, the  
56 “stumpy” bloodstream trypanosome transforms into the procyclic stage within the midgut  
57 lumen [1]. During this process, the coat of variant surface glycoproteins (VSG) is replaced by  
58 a different one composed of procyclins [2, 3]. In the most accepted model of parasite migration  
59 within the tsetse, procyclic trypanosomes first establish an infection in the ectoperitrophic  
60 space (ES) (defined as the space between the gut epithelium and the peritrophic matrix (PM)  
61 Fig. 1a), followed by colonisation of the proventriculus (also known as cardia), and terminating  
62 in the salivary glands, where the parasites become mammalian infective again [4-6].

63

64 The tsetse PM functions to compartmentalise the bloodmeal and to prevent both abrasion and  
65 infection of the gut epithelium [7], thus acting as a protective barrier that trypanosomes must  
66 overcome in order to reach the ES. *Glossina morsitans* secretes a type II PM, which is  
67 continuously produced at a rate of approximately 1 mm/h [8, 9] as an unbroken, multi-layered  
68 concentric sleeve (becoming fully formed after ~80-90h of being secreted [10]) by specialised  
69 cells in the proventriculus. This immunologically important organ [11], marks the border  
70 between the ectodermal foregut (i.e. buccal cavity, pharynx, oesophagus and crop) and  
71 entodermal midgut, functioning as a valve due to its arrangement into a ring-shaped fold  
72 (valvular cardiaca) [12] (see also Supplementary Fig. 1). After secretion, the tsetse PM is  
73 assembled as a trilaminar sheath (PM1-3) [13] (Supplementary Fig. 2), with each layer  
74 differing in thickness and composition, but mainly comprised of chitin fibres that are cross-  
75 linked to structural glycoproteins (peritrophins) [13-15].

76

77 Several suggestions have been made for how trypanosomes reach the tsetse ES, including  
78 circumnavigation of the PM in the posterior gut [16, 17], penetration of the 'freshly secreted'  
79 PM within the proventriculus [18-21], or direct penetration of the 'mature' PM within the anterior  
80 midgut [22-25]. The latter hypothesis, which involves 1) parasite recognition to, and  
81 penetration of, PM1 layer (which faces the gut lumen; Fig. 1a), 2) direct crossing of PM2 and  
82 PM3 layers, and 3) exit to the ES, has persisted for over 40 years and has been influenced  
83 mainly by the visualisation of 'penetrating' trypanosomes between PM layers [22]. However,  
84 neither an adhesion ligand on PM1 has been identified nor has experimental evidence for  
85 steps 2 and 3 been obtained. Moreover, unlike parasites such as *Leishmania* [26] and  
86 *Plasmodium* [27], trypanosomes do not secrete PM-degrading enzymes such as chitinases  
87 [28]. Overall, this suggests that the fast turnover of a structurally complex tsetse PM would  
88 make a difficult barrier for trypanosomes to degrade, although, very little is known about the  
89 physiological response of type II PMs to oral pathogens [29, 30].

90

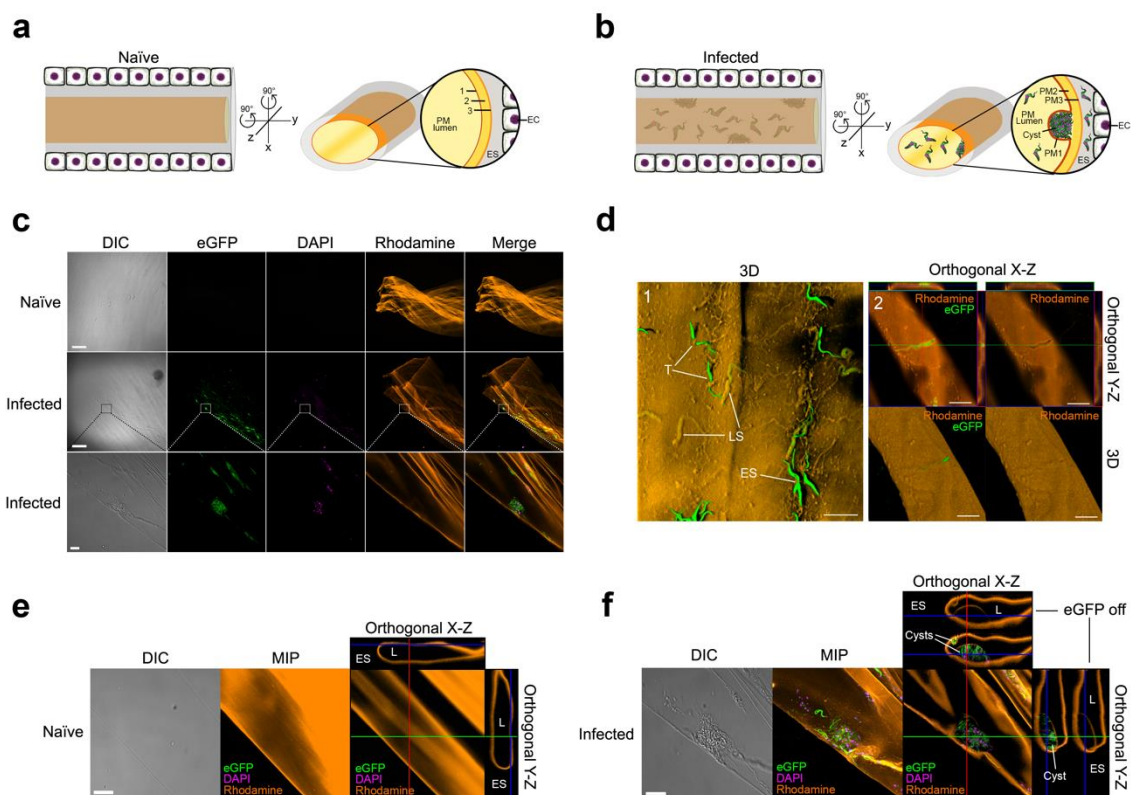
91 In this work, we have revisited how *T. brucei* reaches the tsetse ES by employing several  
92 microscopy techniques, including serial block-face scanning electron microscopy (SBF-SEM),  
93 and novel confocal laser scanning microscopy (CLSM) methodologies, which collectively  
94 allowed the 3D-reconstruction of trypanosome-infected tsetse tissues. We propose that ES  
95 invasion occurs via the proventriculus during PM assembly rather than by direct crossing of  
96 the mature PM in the midgut, as previously suggested [22, 24, 25]. Furthermore, we give  
97 evidence that an early proventricular invasion by trypanosomes is promoted by unknown  
98 factor(s) present in trypanosome-infected blood, thus leading to a higher prevalence of salivary  
99 gland infections and potentially increasing parasite transmission.

100

## 101 **Results and Discussion**

### 102 **CLSM shows trypanosomes are trapped within the tsetse PM**

103 In order to visualise how trypanosomes interact with the tsetse PM, we analysed by CLSM *ex*  
104 *vivo* PMs stained with rhodamine-conjugated wheat germ agglutinin (WGA) [31] from either  
105 naïve flies or flies infected with eGFP-expressing trypanosomes ( $n=35$ ) (Fig. 1 and  
106 Supplementary Videos 1 and 2). WGA exclusively recognises the PM chitin fibres as shown  
107 by its inhibition with chitin hydrolysate or when tissues were stained with the succinylated lectin  
108 (not shown). Whilst individual trypanosomes appear to be partially penetrating the PM or stuck  
109 on either the ES or the luminal side (Fig. 1d), z-stacks orthogonal projections depicted many  
110 parasites inside PM cysts as the rhodamine signal could be seen above and below the cells  
111 (Fig. 1f). This is better visualised when the eGFP signal is switched off. Moreover, the integrity  
112 of all PM cysts analysed was never compromised (i.e. no evidence of parasites penetrating  
113 any of the PM layers) and their thinner part (i.e. PM1, see EM section) always faced the luminal  
114 side.  
115



116

117 **Fig. 1 | CLSM reveals trypanosome cysts formed between PM layers.**

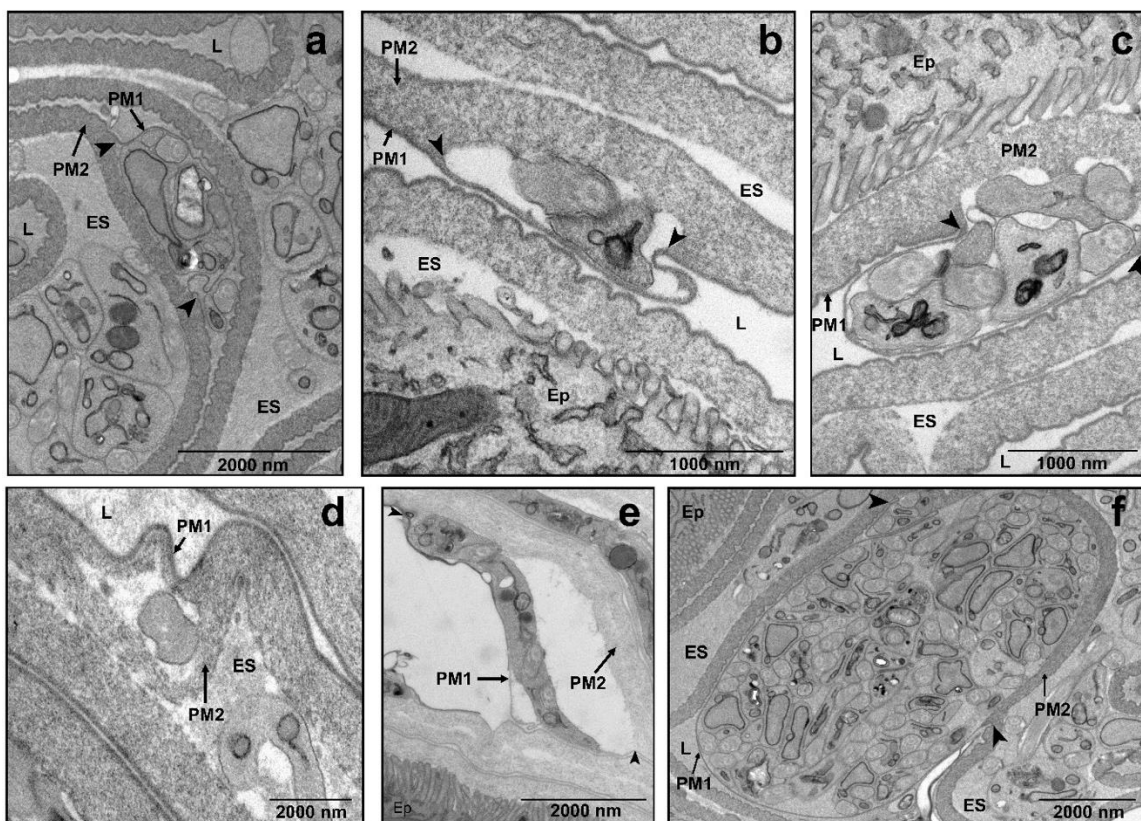
118 **a**, Cartoon depicting a 2D view of naïve tsetse midguts. Rotating 90° on both the X and Y axis gives an  
119 indication of what can be seen under CLSM and provides a guide for understanding the orientation of  
120 the *ex vivo* PMs in the orthogonal view. **b**, Same as Fig. 1a but depicting a section of a trypanosome-  
121 infected gut. Although the three PM layers cannot be seen under CLSM, this schematic shows the  
122 position of the trypanosome cysts between PM1 and PM2; these cysts always orientate towards the  
123 luminal side of the gut (see also Fig. 2). ES, ectoperitrophic space. EC, epithelial cell. **c**, Washed, *ex*  
124 *vivo* PM from a naïve fly (11 dpi) stained with WGA (top). In infected flies (11 dpi), eGFP-trypanosomes  
125 can be seen (green) in close proximity to the PM, with DAPI (magenta) showing parasite nuclei and  
126 kinetoplasts (middle). Scale bar 200µm. Inset corresponds to the higher magnification of the same area  
127 as seen in bottom panel. DIC, Differential Interference Contrast. Scale bar 20µm. **d**, (1) CLSM 3D  
128 reconstructions from multiple z-stacks of washed *ex vivo* PMs from a fly at 9 dpi. Ectoperitrophic space  
129 side (ES), luminal side (LS), trapped trypanosomes (T). Scale bar 20 µm. (2) Maximum Intensity  
130 Projection (MIP) (top) and 3D reconstruction (bottom) of a trapped trypanosome. **e**, A PM sample from  
131 a naïve fly depicting how this tissue looks under DIC and MIP after rendering from multiple z-sections,  
132 whilst the orthogonal view shows the XZ/YZ planes of the folded PM section. **f**, DIC and MIP of an  
133 infected PM sample containing trypanosome cysts, whilst the orthogonal XZ-YZ views show  
134 trypanosomes trapped within PM layers. A second, smaller cyst-like structure can be seen in the XZ  
135 orthogonal view at a North-West position to the bigger cyst. ES, ectoperitrophic space. L, lumen. Scale  
136 bar 20µm.

137

### 138 **Transmission electron microscopy (TEM) analyses of trypanosome-infected midguts**

139 TEM was then used to better understand, at the ultrastructural level, the nature of the PM  
140 cysts and the overall localisation of parasites in infected midguts. We initially focused on the  
141 anterior midgut as previous work suggested trypanosomes may cross the PM in this region  
142 [22-25]. Parasites were observed either in the lumen, trapped within PM layers or already in  
143 the ES at all time-points (5, 8 and 11 dpi). In most infected flies, PM damage was a common  
144 occurrence, which was typically characterised by a separation of PM1 and PM2 layers (Fig.  
145 2a-c, e, and f), as previously reported [22-24]. PM1 appears as a thin (electron-dense) layer  
146 that is equivalent to the luminal rhodamine signal observed by CLSM (Fig. 1f). Furthermore,

147 this damage was not observed in naïve or refractory flies (not shown), and usually one or more  
148 trypanosomes were found within this separation. Occasionally, parasites were seen  
149 embedded within PM2 rather than ‘unzipping’ PM1 from PM2 (Fig. 2d). Moreover, at 11 dpi,  
150 multiple parasites were commonly found between PM layers, forming bigger cysts (Fig. 2f).  
151 The presence of trypanosome-filled cysts, which were more commonly observed in older  
152 infected flies, agrees with the structures observed by CLSM (Fig. 1b and d) and previous  
153 observations [25, 32]. Interestingly, in all instances where PM1 separated from PM2, we found  
154 no evidence of breaks, degradation or thinning of PM1, even when cysts appear to contain  
155 high parasite numbers (Fig. 2f). Furthermore, we never observed parasites in the process of  
156 entering or leaving the PM1 or PM2 side, partially in or out of the PM, nor did we see a  
157 complete break through PM2 layer.  
158



159  
160 **Fig. 2 | TEM images of sections showing trypanosomes between tsetse PM layers.** Typical  
161 damage found in infected flies is the separation of PM1 from PM2. Usually, the electron dense (PM1)  
162 layer appears unbroken, but can be seen peeling away from the second layer (arrowheads). Note that

163 PM1 remains unbroken even when cysts contain high parasite numbers (**f**). Images were taken from  
164 flies at 11 dpi (**a-c**, and **f**), 8 dpi (**d**) or 5 dpi (**e**). L, lumen. ES, ectoperitrophic space. Ep, epithelial cells.  
165 Numbers of technical and biological replicates used, average number of grids and average number of  
166 images per separate grid can be seen in Supplementary table 1.

167

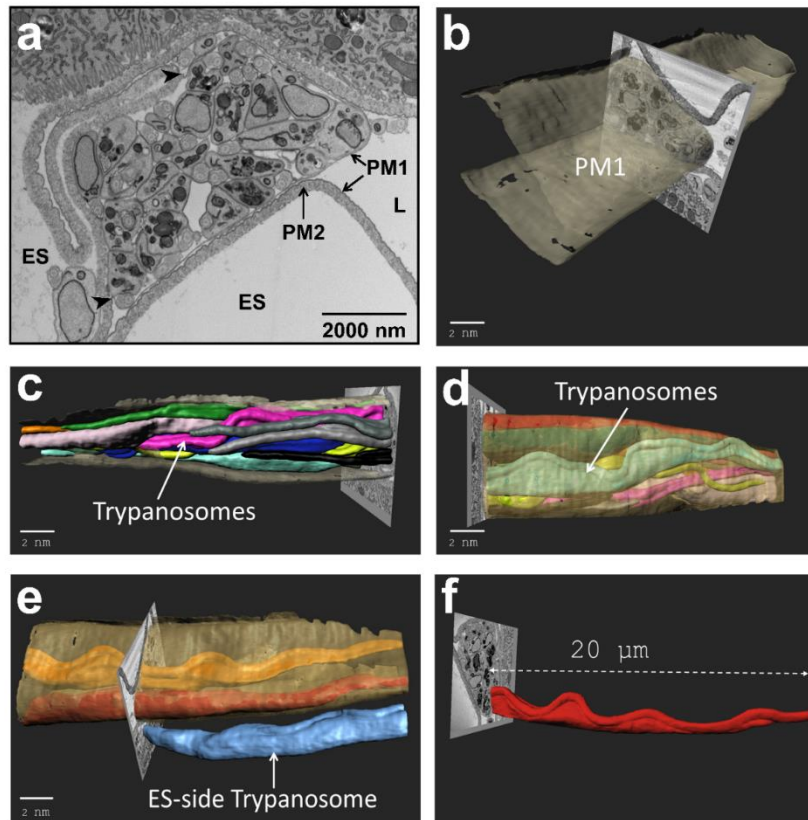
168 **SBF-SEM analysis of a trypanosome cyst reveals conserved parasite orientation and**  
169 **absence of PM degradation**

170 To gain more insights into the organisation of trypanosomes within PM cysts located in the  
171 anterior midgut, we used SBF-SEM. We prepared >500 serial sections (each ~100nm thick)  
172 of a cyst sample (from a fly at 11 dpi) and then 3D-reconstructed this region (Fig. 3,  
173 Supplementary Video 3 and 4). It was observed that all parasites, which appeared to be  
174 aligned in the same direction as indicated by the orientation of the flagellar tips, were  
175 exclusively contained within PM1 and PM2 (Fig. 3c). However, no evidence of crossing or PM  
176 damaged induced by trypanosomes was seen corroborating the CLSM and TEM observations  
177 (Fig. 1 and Fig. 2).

178

179 Why most trypanosomes trapped within the cyst (Fig. 3) appear to have the same orientation  
180 is unknown, particularly when there is no evidence of cell duplication (e.g. flagellar division) in  
181 this and other cysts that were analysed by TEM. Alternatively, we hypothesise that  
182 proventricular parasites may form cysts by collective motion (CoMo) [31] whereby several  
183 trypanosomes, swimming in the same direction, may simultaneously penetrate through an  
184 immature PM thus becoming trapped between its layers.

185



186

187 **Fig. 3 | SBF-SEM 3D reconstruction of a trypanosome cyst in the PM from the anterior midgut.**

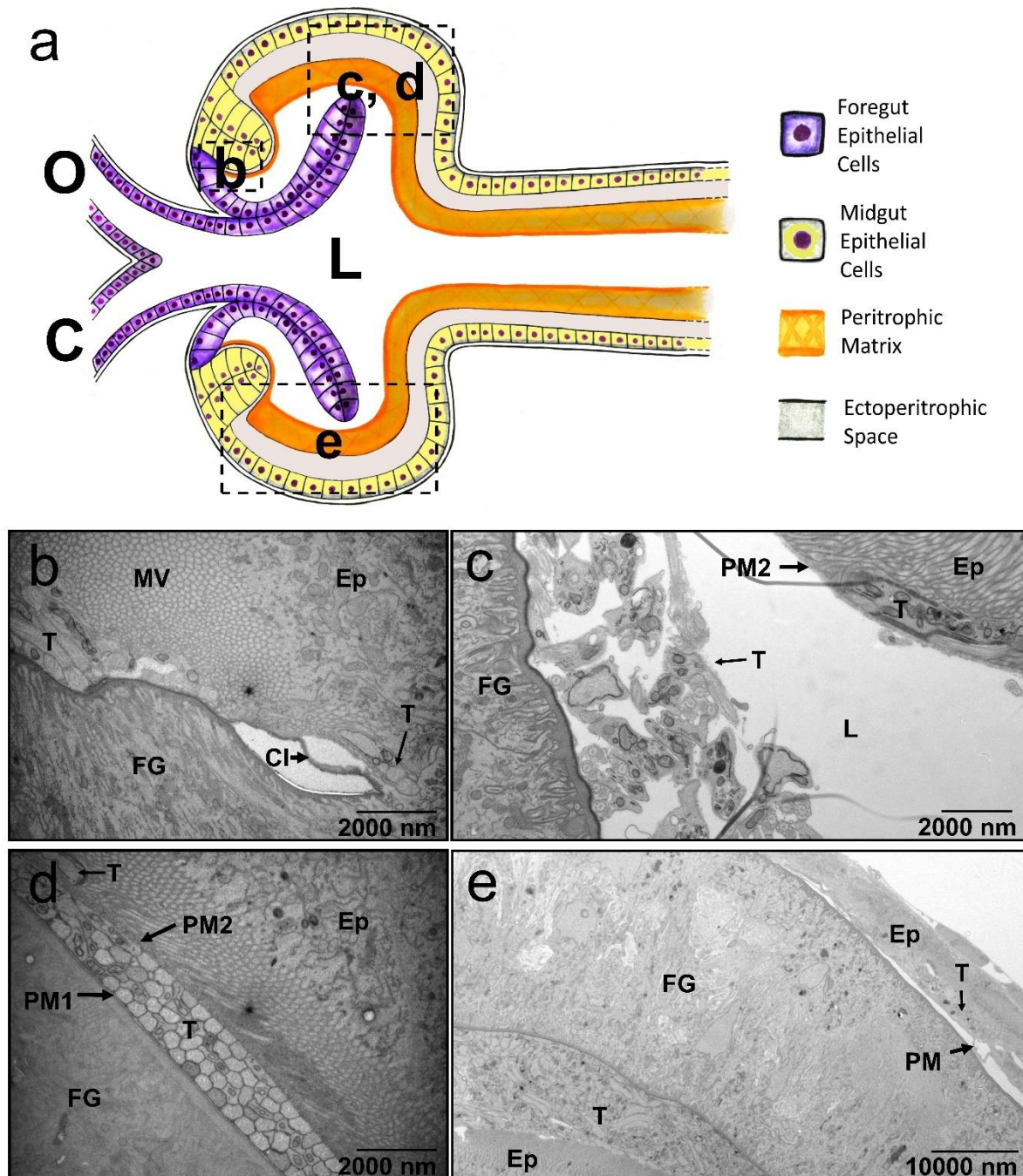
188 Sample taken from a fly at 11 dpi. See also Supplementary Video 4. **a**, Multiple trypanosomes between  
189 PM1 and PM2. Arrows show the point of separation as trypanosomes reside inside and both layers  
190 remain unbroken. ES, Ectoperitrophic Space. L, Lumen. **b-e**, SBF-SEM slices merged with manual  
191 segmentation. **b**, Image illustrating breaks or damage to PM1 (grey) are absent during a trypanosome  
192 infection. **c**, Multiple parasites between PM1 and PM2; most parasites appeared oriented in the same  
193 direction as indicated by the position of the anterior end flagellar tips. **d**, A reverse view of the image  
194 depicted in 4c, showing parasites contained within PM1. **e**, Still depicting one parasite (blue) in the  
195 ectoperitrophic space side. **f**, A measurement of a partially reconstructed trypanosome within the cyst.  
196 Scale bars are representative of the SEM image (not the reconstruction).

197

### 198 **Trypanosomes reach the ES by early invasion of the proventriculus**

199 The fact that none of the trypanosomes inside the reconstructed cyst or the ones observed by  
200 either TEM or CLSM appear to penetrate the PM layers was puzzling. This raises the question  
201 of how these cysts are formed if no evidence of parasite crossing is seen in the anterior midgut.

202 One clue, however, came from the lengths of individual trypanosomes from inside the (3D-  
203 reconstructed) cyst, which were longer than average midgut procyclics (~20µm; see example  
204 in Fig. 3f) and so similar in size to mesocyclic proventricular forms [31, 33] (see also Fig. 7).  
205 Therefore, we hypothesised that trypanosome-containing cysts could originate in the  
206 proventriculus during PM assembly and consequently, analysed the proventriculus from  
207 infected flies at 5 (early infection, Fig. 4) and 11 (late infection, Fig. 5) dpi. After 5 dpi, the  
208 proventriculus was heavily infected (63.6% prevalence) with trypanosomes (Fig. 4b-e).  
209 Parasites were observed to be adjacent to where the foregut cells become confluent with  
210 midgut cells. This suggests trypanosomes can overcome or bypass the PM at this point (Fig.  
211 4b), confirming previous observations [18-21]. Parasites were also observed in the lumen and  
212 ectoperitrophic side of the PM and, in some cases, in close proximity to (but not penetrating)  
213 the epithelial cells. Moreover, they could also be seen between PM1 and PM2 (Fig. 4d). A  
214 proventriculus from a fly at 5 dpi (Supplementary Fig. 3) was subsequently processed for SBF-  
215 SEM at the regions of interest (ROI) shown (Supplementary Video 5 and 6), and a partial  
216 reconstruction of a small number of parasites that were in close proximity to the chitinous  
217 foregut was performed on ROI 2 (Supplementary Video 7).

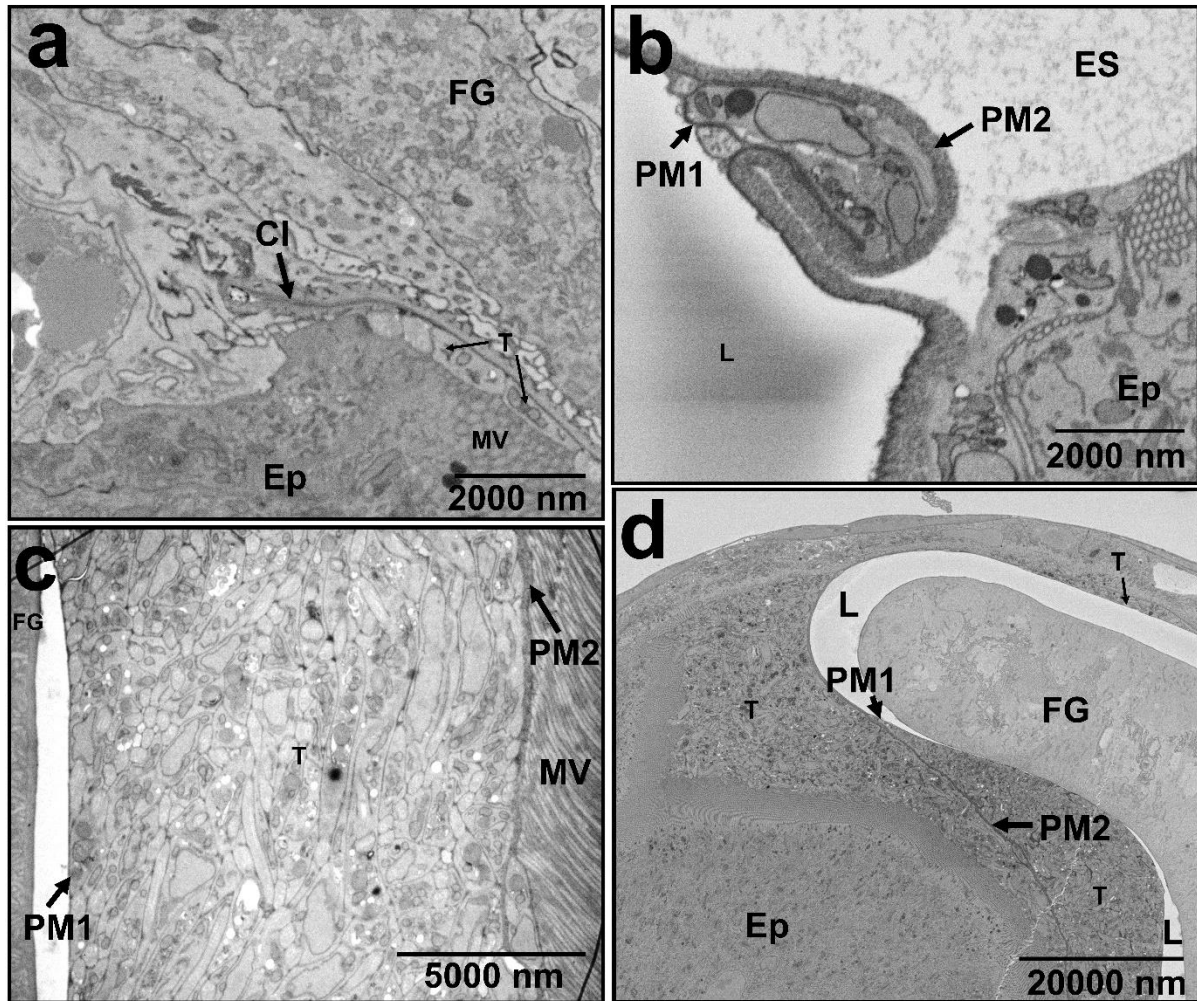


226 between the foregut (FG) and the proventricular/midgut epithelial cells (Ep). Trypanosomes (T) can  
227 already be seen near to the epithelial cells. CI, Cuticular Intima. MV, microvilli (8200 x). **c**, Only PM2 is  
228 visible and trypanosomes appear to be filling the cavity between the foregut and epithelial cells (8200  
229 x). **d**, Tightly packed parasites can be seen already trapped between PM1 and PM2, and a single  
230 trypanosome (T) can also be seen already in the ES (8200 x). **e**, The proventriculus is heavily infected,  
231 and parasites are located in the lumen, the ES and between PM layers (1700 x). All midguts from the  
232 same proventriculus samples shown in this figure had trypanosome infections (not shown).

233

234 At 11 dpi, trypanosomes continued to be seen in the proventriculus (Fig. 5) (50% prevalence).  
235 However, whilst at 5 dpi parasites were located in the ES, the lumen and also between PM  
236 layers, by 11 dpi trypanosomes were neatly contained either within PM layers or inside the ES  
237 (Fig. 5c-d). In addition, cyst-like structures such as those in the anterior midgut could be  
238 observed (Fig. 5b) and with no evidence of a damaged PM1 layer. In summary, at 5 dpi, flies  
239 show two clear phenotypes: susceptible – those that have a high parasite load (including  
240 trypanosomes near to the cuticular intima of foregut cells) and refractory – those with no sign  
241 of parasite infection. In the former, trypanosomes widely distribute throughout the  
242 proventriculus, filling all available spaces. The high parasite numbers indicate trypanosomes  
243 are replicating during early infection. In contrast, by 11 dpi, parasites are absent from the  
244 proventriculus lumen and concentrated within PM layers. Overall, TEM analyses of infected  
245 proventriculi suggest trypanosomes are capable of penetrating the PM at its point of synthesis.  
246 Here PM2 is not fully formed and exists as a disorganised structure [21], so it is possible for  
247 trypanosomes to become passively engulfed by it rather than actively penetrating as  
248 previously suggested.

249



250

251 **Fig. 5 | Proventricular trypanosomes contained within the PM and formation of trypanosome-**  
252 **filled cysts at 11 dpi.** Micrographs are taken from an equivalent area of the proventriculus as shown  
253 in Fig. 5. **a**, Area of cell transition between the foregut (FG) and the epithelial cells (Ep). Trypanosomes  
254 (T) can already be seen near to the epithelial cells. CI, Cuticular Intima. MV, microvilli (8200 x). **b**, Cysts  
255 of trypanosomes are formed in the proventriculus (8600 x). **c**, Trypanosomes neatly contained in the  
256 ES with no visible parasites in the lumen (L). Parasites can also be seen between PM1 and PM2 (1700  
257 x). **d**, High numbers of parasites (T) can be seen trapped between PM1 and PM2 layers, and within the  
258 ES (8600 x).

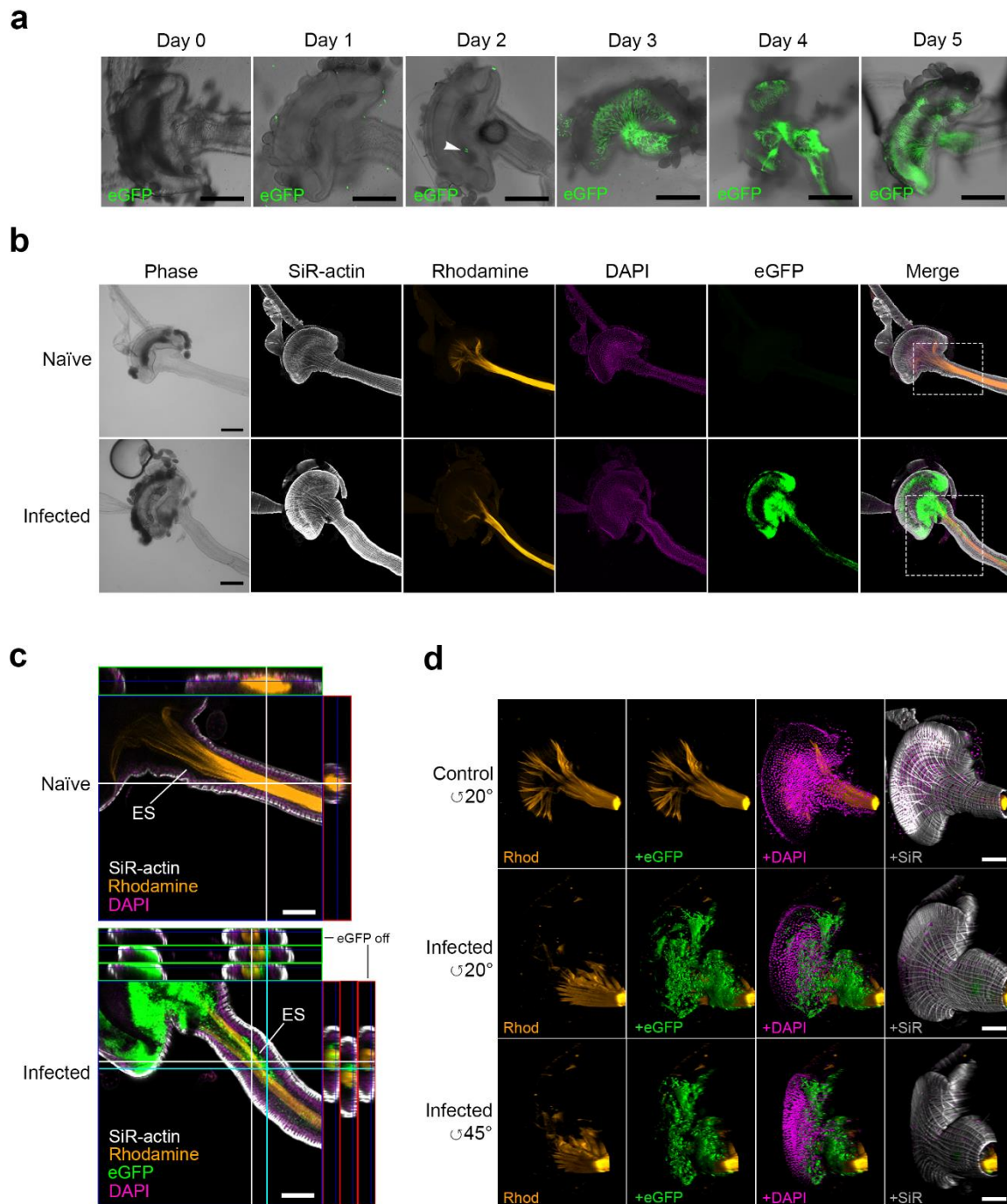
259

### 260 **CLSM confirms early proventricular colonisation**

261 To further demonstrate an early proventricular invasion by trypanosomes, we used CLSM to  
262 localise live parasites (eGFP-expressing J10 BSFs, one of the strains used for TEM analysis)  
263 within tsetse tissues over a 5-day time course (Fig. 6). This parasite strain expresses eGFP

264 only upon transformation into procyclics. Trypanosomes were detected within the  
265 proventriculus from 2 dpi (10% infection prevalence) onwards; however, at 3 dpi  
266 (Supplementary Fig. 4), heavy proventricular infections could be seen in 35% of the flies.  
267 Additionally, most of the flies at 3-5 dpi presented a high midgut infection particularly in the  
268 anterior midgut, either within the ES or the midgut lumen (Fig. 6a and 6d, and Supplementary  
269 Videos 8, 11 and 12).

270



271

272 **Fig. 6 | CLSM analysis of the early proventricular infection by bloodstream trypanosomes.** **a**, Time  
 273 course of infection up to 5 dpi with eGFP BSFs J10 strain. Figure shows representative proventriculi  
 274 and anterior midguts from each dpi. "Day 0", proventriculus from a fly dissected 1h after receiving an  
 275 infected meal. White arrowhead at 2 dpi shows trypanosomes within the proventriculus (see also  
 276 Supplementary video 8). Scale bar 200  $\mu$ m under 10X. **b**, Example of an infected proventriculus and

277 anterior midgut (3 dpi) showing the location of trypanosomes (green) in relation to the PM (orange). Top  
278 panel, naïve flies (Supplementary videos 9 and 10). Both naïve and trypanosome-infected flies received  
279 serum meals containing rhodamine-WGA four hours prior to dissection, which shows PM originating  
280 from proventriculus. SiR-actin labels the filamentous-actin (white) of all tsetse proventricular cells and  
281 DAPI (magenta) their nuclei. Bottom panel, a heavy trypanosome infection inside the proventriculus  
282 and anterior midgut (Supplementary videos 11 and 12). Insets were analysed at a higher magnification  
283 (6c). Scale bars 100  $\mu$ m under 10X. **c, top**, Representative stack from a 3D-reconstructed  
284 proventriculus and anterior midgut at the region of interest from a naïve fly. Scale bar 100  $\mu$ m under  
285 10X. **c, bottom**, Representative stack from a 3D-reconstructed infected proventriculus and anterior  
286 midgut. Trypanosomes can be seen in the ES within either the proventriculus or the anterior midgut,  
287 whilst the orthogonal views show trypanosomes either within the lumen or the PM layers (white section),  
288 or within the ES (cyan section). Scale bar 100  $\mu$ m under 10X. **d**, CLSM 3D reconstructions from multiple  
289 z-stacks of proventriculi and anterior midgut from a naïve (top) and infected fly at 5 dpi (middle and  
290 bottom). Scale bar 100  $\mu$ m under 10X.

291

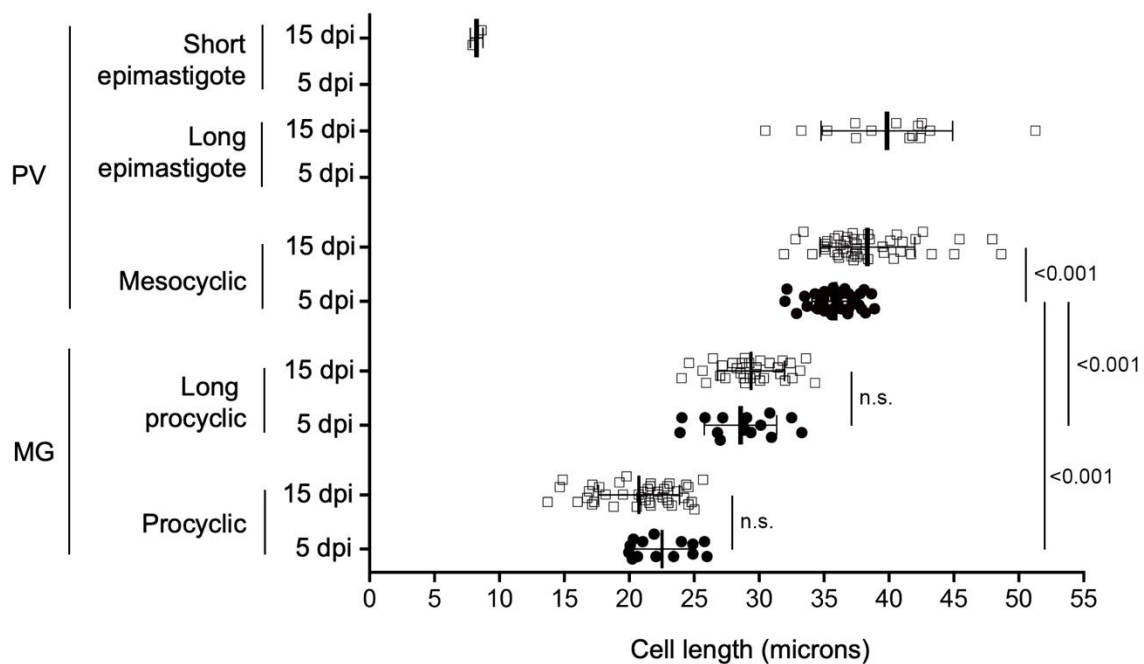
292 The same early proventricular infection phenotype was also seen in flies infected with BSFs  
293 from another *T. b. brucei* strain (AnTat 1.1, clone 90:13) (Supplementary Fig. 5a). However,  
294 and completely unexpected, when infections were carried out using *in vitro* cultured AnTat 1.1  
295 BSFs (cBSF) proventricular trypanosomes could only be seen at 15 dpi or later  
296 (Supplementary Fig. 5a-b). Furthermore, the ability of cBSFs to colonise the proventriculus  
297 few days after infection was severely reduced as early as 9 days after adaption in culture when  
298 compared to BSFs (Supplementary Fig. 5a). Strikingly, whilst BSFs are able to establish  
299 normal salivary gland (SG) infections (21% infection prevalence), recently adapted cBSFs  
300 show lower prevalence (10%) and cBSFs completely fail (0%) to colonise the tsetse SGs  
301 (Supplementary Fig. 5a). Furthermore, when we retrospectively analysed infection data  
302 collected in our lab over a period of three years, it was confirmed that almost 30% of flies fed  
303 with AnTat BSFs developed SG infections (Supplementary Fig. 5c). In contrast, flies that  
304 received bloodmeals containing either procyclic or cBSFs produced ~10% and 0% SG  
305 infections, respectively, after 30 days. Thus, an early proventricular colonisation by

306 bloodstream trypanosomes results in a higher infection prevalence of the tsetse salivary  
307 glands.

308

309 To understand the dynamics of trypanosome development in early proventricular infections,  
310 we isolated parasites from infected proventriculi and midguts at 5 and 15 dpi, and analysed  
311 length (Fig. 7), morphology, and kinetoplast position relative to the nucleus [4, 31, 33]  
312 (Supplementary Fig. 6). Proventricular trypanosomes at 5 dpi, although on average  $\sim 3\mu\text{m}$   
313 shorter in length than those observed at 15 dpi, were significantly longer ( $\sim 35\mu\text{m}$  average  
314 length) and morphologically different than midgut procyclics, at either time point. This implies  
315 procyclic forms can differentiate into mesocyclics early on within the proventriculus.  
316 Epimastigote forms developed at a slower rate and were only detected from 15 dpi.

317



318

319 **Fig. 7 | Analysis of trypanosome life stages at different infection times and tsetse tissues.**

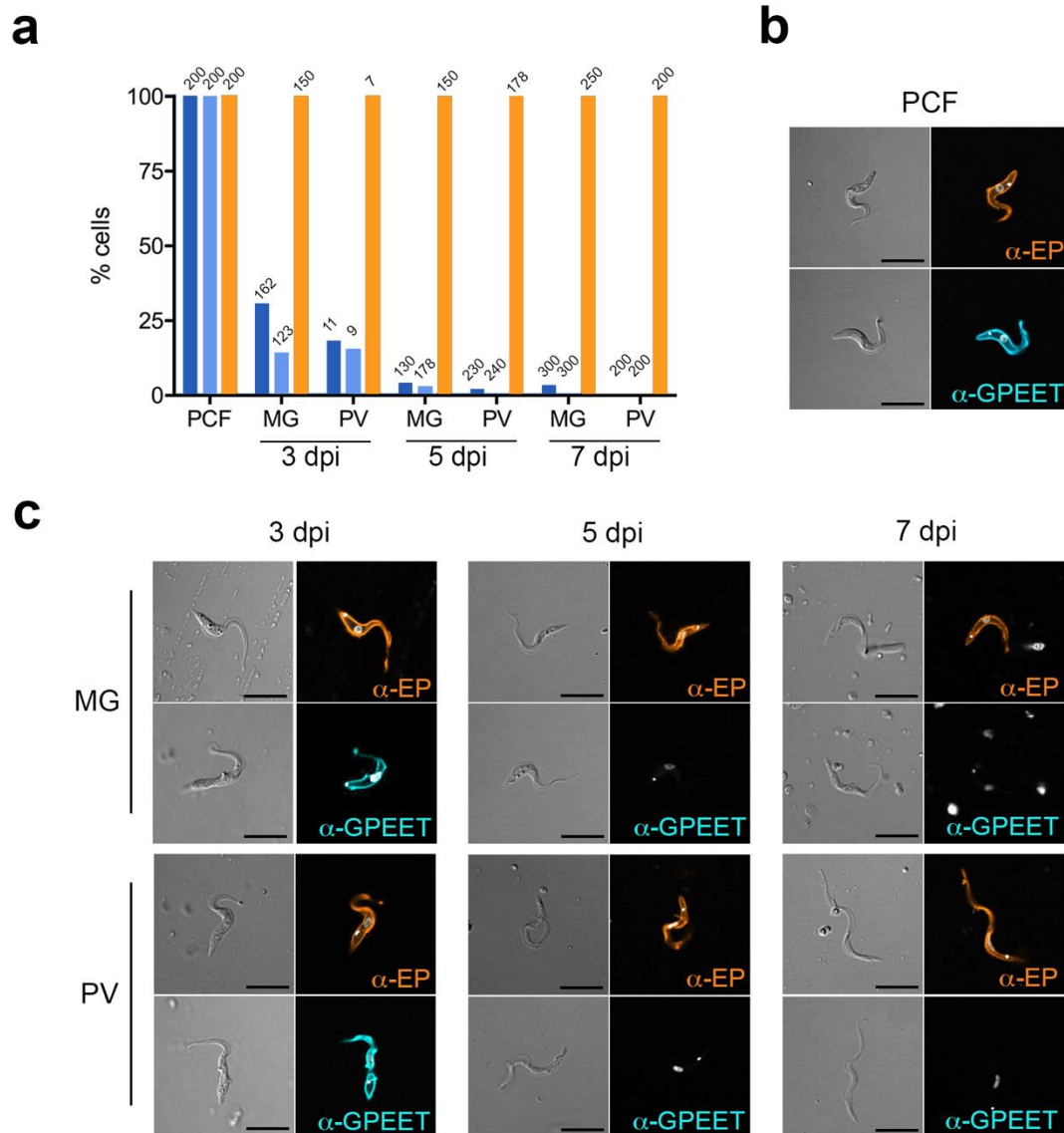
320 Mean cell length ( $\mu\text{m}$ ) of trypanosomes isolated from fly midguts (MG) and proventriculi (PV) at either  
321 5 dpi (●) or 15 dpi (□) were DAPI stained and analysed by CLSM. Midgut trypanosomes include free  
322 swimming and encysted parasite forms. Error bars represent  $\pm$  s.d. Vertical lines show statistical

323 significance (one-sided *t*-test, assuming normal distribution) among life stage groups and the two time  
324 points (p-values indicated next to vertical lines).

325

326 We also compared the expression of procyclin, a surface glycosylphosphatidylinositol (GPI)-  
327 anchored glycoprotein marker, in proventriculus and midgut trypanosome populations using  
328 antibodies specific for each form (EP or GPEET; Fig. 8) [34]. We observed a similar pattern of  
329 procyclin expression in parasites isolated from both organs at 3, 5 and 7 dpi. Whilst EP  
330 procyclin was detected in 100% of cells at all time points, both forms of GPEET  
331 (unphosphorylated and phosphorylated) were primarily detected in proventricular and midgut  
332 forms at 3 dpi. Altogether, these results suggest that although proventricular trypanosomes  
333 may be developing at a faster rate than those in the midgut, the programme of procyclin  
334 expression mirrors that of proliferating midgut procyclics; i.e. GPEET is only expressed early  
335 on during the infection (regardless of the trypanosome stage and tissue infected) and EP  
336 becomes the dominant form from 5 dpi onwards [2, 3]. Interestingly, at 3 dpi, midgut  
337 trypanosomes showed a fully posterior kDNA compared to proventricular forms at the same  
338 time-point (Fig. 8c), which is more reminiscent of transforming 'stumpies' than fully developed  
339 procyclic cells.

340



341

342 **Fig. 8 | *T. brucei* procyclin expression during early infection in the tsetse.** **a**, Profile of procyclin

343 expression in trypanosomes during a time course infection experiment ( $n=1$ ) as determined by

344 immunostaining. Percentage of *T. brucei* cells from midgut (MG) and proventriculus (PV) at 3, 5 and 7

345 dpi, either recognised by antibodies against GPEET (phosphorylated (dark blue) or unphosphorylated

346 (light blue)) or EP procyclins (orange). Numbers on bars represent individual trypanosomes analysed.

347 **b**, Representative immunostaining images of *T. brucei* procyclic cultured forms (PCF) (antibody

348 controls) shown in differential increased contrast (left) and a merged image of DAPI DNA counterstain

349 (white) with either anti-EP (orange) or anti-GPEET (phosphorylated; blue) (right). **c**, >100 cells per

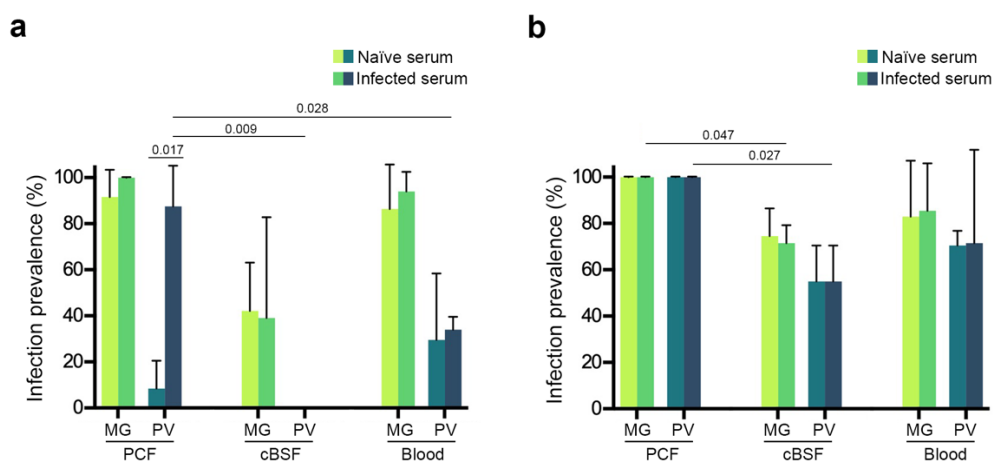
350 tissue and time point were analysed for each antibody with the exception of cells from the PV at 3 dpi

351 due to very few infections at this time ( $n=11$ , 9 and 7 for phosphorylated GPEET, unphosphorylated  
352 GPEET and EP, respectively). Imaged at 63X; Scale bars 10 $\mu$ m.

353

### 354 **Do serum factors influence early colonisation of the proventriculus?**

355 We also investigated whether factors in trypanosome-infected serum promoted an early  
356 proventricular colonisation (Fig. 9). Teneral flies that received bloodmeals consisting of  
357 established AnTat 1.1 90:13 cBSFs, spiked with either naïve serum or serum from mice  
358 originally infected with BSFs AnTat 1.1 90:13, showed no proventricular colonisation  
359 compared to BSFs at 5 dpi (i.e. >30% infection prevalence; Fig. 9a). Infectivity was only  
360 evident at 10 dpi (Fig. 9b). Surprisingly, flies that were fed with bloodmeals consisting of AnTat  
361 1.1 90:13 procyclic cultured forms (PCFs) spiked with infected serum showed a significant  
362 10.3-fold increase in proventriculus infection prevalence (>87% average) at 5 dpi compared  
363 with the control serum group. This suggests that serum factors from trypanosome-infected  
364 blood may facilitate early proventricular infections only once transformation from BSFs into  
365 PCFs has occurred within the fly gut. However, these results also indicate that intrinsic cell  
366 factors are important to establish an early proventricular infection as this phenotype was lost  
367 during long-term culture and could not be rescued in the presence of trypanosome-infected  
368 serum (Fig. 9a).



369

370 **Fig. 9 | *T. brucei* life stages display different infection phenotypes in the fly when in the presence**  
371 **of serum from trypanosome-infected animals. Mean trypanosome infection prevalence (percentage)**

372 in midguts and proventriculi of tsetse infected with bloodmeals consisting of serum harvested from either  
373 trypanosome-infected blood or naïve and then equally combined with washed parasites (either cultured  
374 procyclics forms (PCFs), cultured bloodstream forms (cBSFs) or bloodstream forms from infected mice  
375 (BSFs)) and horse blood, were given to teneral flies and then infection prevalence was scored after 5  
376 (a) or 10 (b) dpi. Error bars show  $\pm$  s.d. Horizontal lines represent statistical significance from two  
377 biological replicates ( $n=2$ ) using a one-sided *t*-test assuming normal distribution (p-values indicated on  
378 the lines).

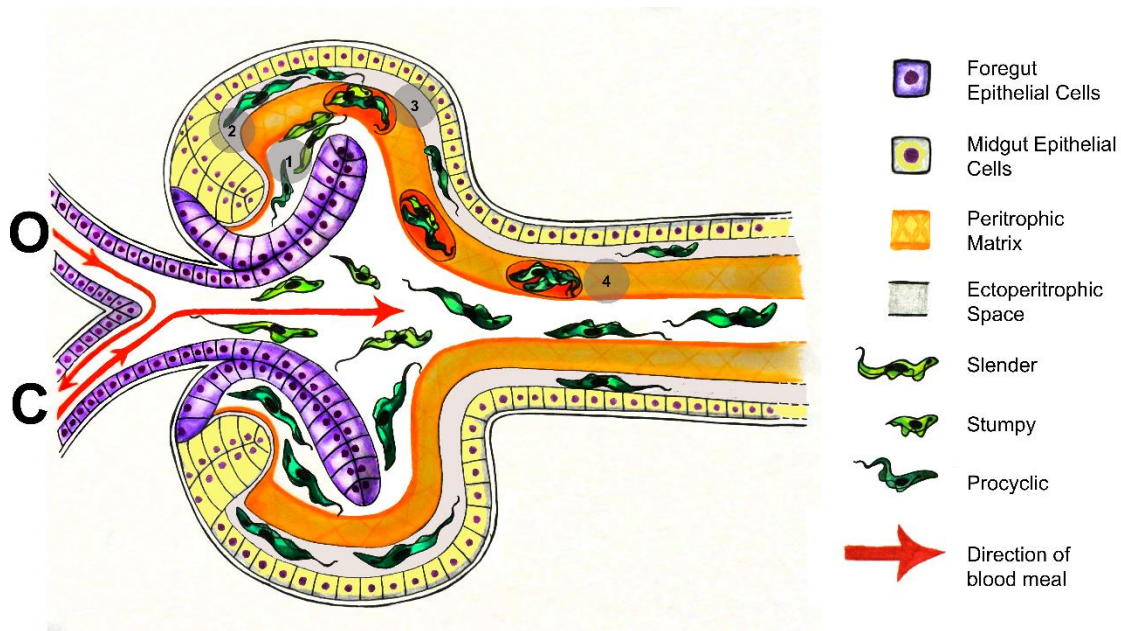
379

380 One possible serum factor that could promote establishment of an early proventricular  
381 infection are released variable surface glycoproteins (VSGs) [35-39]. However, when flies  
382 were infected with Antat 1.1 PCFs in bloodmeals containing several concentrations of soluble  
383 (i.e. GPI-cleaved) VSG variant MITat1.4, we saw no significant difference in either  
384 proventricular or midgut infectivity (data not shown). It is worth mentioning that upon ingestion  
385 of a trypanosome-infected bloodmeal, released VSG molecules –presumably from  
386 transforming parasites– lead to a transcriptional down-regulation of PM associated genes  
387 expressed by proventricular epithelial cells, including several peritrophins [29]. The authors  
388 conclude that this interference facilitates the crossing of the PM by procyclic trypanosomes in  
389 the anterior midgut during early infection. However, based on the data herein presented, we  
390 suggest that the VSG-induced down-regulation of proventricular genes may instead facilitate  
391 parasite crossing of the PM in the proventriculus rather than in the anterior midgut in which  
392 the PM is present as a fully assembled, multi-layered tissue. Furthermore, whilst at a  
393 transcriptional level this may be true, a comparison of the PM width in the anterior midgut  
394 between naïve and infected flies (at either 5 or 11 dpi) showed no significant difference in  
395 architecture or thickness as evaluated using TEM. On average, the tsetse PM is ~300nm in  
396 all conditions (Supplementary Fig. 7).

397

398 Our results support a new infection model where recently transformed *T. brucei* procyclics  
399 reach the ectoperitrophic space after crossing the peritrophic matrix located within the

400 proventriculus [18, 19], and not in the anterior midgut as previously suggested [22, 24, 25]. In  
401 this scenario, procyclic trypanosomes can either first establish a proventricular infection and  
402 then gradually invade the ES after 3 dpi or, alternatively, directly establish an ES infection in  
403 the anterior midgut and then migrate to the proventriculus as the infection progresses (usually  
404 after one week depending on the parasite strain). The precise location of PM penetration by  
405 trypanosomes within the proventriculus remains unknown; however, we hypothesise that it  
406 may occur in the region where specialised epithelial cells (annular pad) secrete the different  
407 PM layers, as suggested by Fairbairn in 1958 [20] and later by Moloo in 1970 [21]. If so, this  
408 implies a race against time for trypanosomes as they must escape the confines of the PM to  
409 gain entry into the ES before it matures to a point where they become trapped in cysts that  
410 move along the midgut (due to continuous PM secretion) and then become potentially  
411 eliminated in the hindgut (posterior end; Fig. 10). Indeed, TEM analysis of the hindgut from  
412 infected flies showed parasites with abnormal morphology (i.e. containing many intracellular  
413 vesicles and multiple flagella) and a damaged PM (Supplementary Fig. 8), suggesting a  
414 possible degradation as parasite cysts transit towards this region. The remarkable PM  
415 expansion observed in some of the cysts at 11 dpi, where the PM layers remain intact despite  
416 containing several tightly packed trypanosomes, is indicative of a highly flexible PM rich in  $\beta$ -  
417 chitin fibres cross-linked to O-glycosylated peritrophins [14, 40]. Whether parasite  
418 encapsulation within the PM is a novel tsetse defence mechanism to control trypanosome  
419 infection intensity remains to be elucidated, but one should note this process does not lead to  
420 self-cure. In fact, in flies at least 40 dpi, similar cysts have been reported within the  
421 proventriculus in which the integrity of PM1 seems to be compromised, although the  
422 phenotypic differences could be accounted for by fly age and duration of infection [41]. In  
423 summary, the model of trypanosome PM crossing in the anterior midgut, which for several  
424 decades has been mainly supported by TEM visualisation of parasite cysts in the same region  
425 [22], can no longer be accepted as the sole route of ES invasion based on our collective  
426 microscopy evidence.



427

428 **Fig. 10 | Schematic (artistic) representation depicting the entry trypanosomes into the**  
429 **ectoperitrophic space via the proventriculus.** Specialised epithelial cells in the proventriculus  
430 annular pad are responsible for PM (orange) assembly and secretion. Ingested trypanosomes (green)  
431 either remain in the proventriculus lumen (1) successfully migrate to the ES through a more fluid PM in  
432 the proventriculus (2) before it matures into a rigid structure as seen in the midgut, or become trapped  
433 between PM layers (cysts) (3). Those that have become trapped between PM layers are carried through  
434 to the midgut as the PM continues to be secreted (4). "O" and "C" represents direction of the blood flow  
435 from either the oesophagus or crop, respectively.

436

437 Why procyclic trypanosomes 'hide' within the proventriculus and/or midgut ES to establish an  
438 infection is unknown. As previously suggested, the most likely explanation is that the tsetse  
439 ES offers a safer environment to proliferative procyclic trypanosomes against the action of  
440 harmful blood factors, including reactive oxygen species [11, 42] and vertebrate complement  
441 [43]. In addition, considering that the tsetse PM is continually secreted, attachment to it from  
442 the midgut lumen would result in the eventual excretion of trypanosomes. This contrasts to  
443 mechanisms used by *Leishmania* and *Plasmodium* parasites within the gut of the sand flies  
444 and mosquitoes, respectively, as these parasites secrete chitinases to degrade the type I PM  
445 of these insects in order to migrate [26, 27, 44]. Trypanosomes do not secrete chitinases,  
446 however, exochitinase activity from the tsetse symbiont *Sodalis glossinidius* [45] or bloodmeal

447 chitinases [46] may facilitate trypanosomes penetration into the proventriculus. Thus, invasion  
448 of the ES by penetrating an immature PM in the proventriculus may be an adaptive strategy  
449 to compensate for the inability of all *T. brucei* sub-species (and possibly also for *T.*  
450 *congolense*) to attach to and degrade a mature tsetse PM. In fact, a type II PM is a more  
451 complex and organised structure compared to type I PMs, and blood feeding insects secreting  
452 type I PMs are usually more permissive disease vectors [7].

453

454 It is not clear what the impact of an early proventricular colonisation has on trypanosome  
455 development or transmission. Our results indicate that establishment of an early proventricular  
456 infection may increase parasite transmissibility as the proportion of infected SGs is much  
457 higher compared to strains (or parasite stages) that first colonise the midgut. The tsetse  
458 proventriculus, besides regulating the blood flow coming from the oesophagus and crop, and  
459 also being the place of PM synthesis, is an immunoregulator organ that responds to a  
460 trypanosome infection by increasing the levels of nitric oxide and radical oxygen species, and  
461 parasite-specific antimicrobial peptides [11, 47]. Collectively, these molecules appear to be  
462 key in conferring to tsetse refractoriness to a trypanosome infection. Thus, it is possible that  
463 during an early colonisation of the proventriculus, procyclic trypanosomes in combination with  
464 serum factors present in infected blood down-regulate the release of immunoregulator  
465 molecules, which in turn will facilitate establishment of a parasite infection and a faster  
466 development (i.e. formation of epimastigotes) within this organ. This is in contrast to a later  
467 proventricular colonisation phenotype, which normally occurs after 10 dpi and correlates with  
468 a lower transmission index.

469

470 There is increasing evidence that procyclic trypanosomes undergo social motility (SoMo) *in*  
471 *vitro* [48-50]. This phenomenon appears to occur only in early procyclic cells, which are  
472 characterised by expressing GPEET procyclin on the surface [51]. Furthermore, although  
473 SoMo is yet to be observed within the fly's midgut, it may play a role in the migration of midgut

474 procyclics to the proventriculus [52, 53]. We did not investigate whether trypanosome SoMo  
475 occurs *in insecta*, but our data suggest that this phenomenon could happen in developing  
476 (early) procyclics in the proventriculus, as supported by the expression of GPEET procyclins  
477 in proventricular-associated parasites (Fig. 8). Alternatively, there is strong evidence for  
478 trypanosome CoMo within infected tsetse tissues [31], although this may not be operative  
479 during an early proventricular infection. However, both phenomena (SoMo vs. CoMo) are not  
480 necessarily mutually exclusive as they could operate in parallel or at different stages of  
481 trypanosome development in tsetse.

482

483 In conclusion, we have developed new microscopy methodologies that allowed us to revisit  
484 the route by which trypanosomes migrate through the tsetse gut. We provide evidence that *T.*  
485 *brucei* procyclics reach the tsetse ES when they encounter the immature PM secretions at its  
486 point of production in the proventriculus. Furthermore, trypanosomes observed within PM  
487 cysts in the anterior midgut are likely formed in the proventriculus during PM assembly and  
488 are not indicative of PM penetration in this region. Moreover, unknown factors present in  
489 infected blood (of mammalian and/or parasite origin) may promote early proventricular  
490 invasion, which in turn leads to higher salivary gland infection rates and potentially increasing  
491 parasite transmission.

492

## 493 **Materials and Methods**

### 494 **Tsetse**

495 Male flies were reared in an established colony (*Glossina morsitans morsitans* (Westwood))  
496 at the Liverpool School of Tropical Medicine and maintained on sterile, defibrinated horse  
497 blood (TCS Biosciences) at an ambient temperature of 27°C ± 2°C and a relative humidity of  
498 65-75%. Experimental flies were collected at <24 hours post-eclosion (p.e.) and offered a  
499 bloodmeal every 2 days before being starved for 72 hours in preparation for dissection at

500 variable timepoints (5, 8 or 11 dpi) control blood meal. Flies used for CLSM were an exception  
501 to this feeding regime (see below).

502

### 503 **Trypanosome strains**

504 Three different strains of *Trypanosoma* (Trypanozoon) *brucei brucei* were used in this study.  
505 TSW-196 BSFs [54] (from murine stabilates) were used for TEM experiments. J10  
506 (MCRO/ZM/73/J10) green fluorescent protein (eGFP) expressing BSFs [55] were used for  
507 TEM, CLSM and both BSFs and procyclic forms (PCFs) used in the procyclin expression  
508 experiments. BSFs of AnTat 1.1 90:13 engineered with an mNeonGreen expressing construct  
509 was used for CLSM (see below), whilst cultured BSFs (cBSFs) and PCFs of the same strain  
510 was used for CLSM and infected serum experiments. For infections, flies <24 hours p.e. were  
511 fed either a blood or serum meal containing one of the strains described above; unfed flies  
512 were removed and conditions prior to sacrifice are the same as described for control flies.

513

### 514 **Trypanosome growth and transformation**

515 Cultured BSFs were grown in HMI-9 supplemented with 10% foetal bovine serum (FBS) at  
516 37°C with 5% CO<sub>2</sub> whereas PCFs were grown in SDM-79 with 10% FBS at 27°C and 5% CO<sub>2</sub>.  
517 Cultured BSFs were transformed to PCFs using 6mM cis-aconitate in DTM (Differentiation  
518 medium [56]) supplemented with 20% FBS at 27°C and 5% CO<sub>2</sub> for 24 hours. To generate  
519 the trypanosome mNeonGreen clone, 4x10<sup>7</sup> AnTat 1.1 90:13 cultured BSF cells in exponential  
520 growth phase were transfected with 10µg of a modified pALC14 plasmid ([57]) for ectopic  
521 expression of the tetracycline-inducible mNeonGreen protein under a *GPEET* procyclin  
522 promoter, using an Amaxa 4D nucleofector (program FI-115). Clonal cell lines were selected  
523 by limiting dilution in SMD-79 10% FBS, containing 1µg/mL puromycin.

524

### 525 **Transmission Electron Microscopy**

526 Tsetse midguts or proventriculi were dissected in ice-cold fixative (0.2M cacodylate, 4%  
527 paraformaldehyde (PFA), 2.5% glutaraldehyde (GA), 3% sucrose, pH 7.4), transferred to fresh  
528 fixative, and incubated on ice for an hour. Tissues were then washed twice in ice-cold 0.1M  
529 cacodylate buffer containing 3% sucrose (pH 7.4) for 2 minutes and left in 1% osmium  
530 tetroxide for an hour at room temperature. After washing with copious amounts of ice-cold  
531 0.1M cacodylate buffer, followed by washes with distilled water, tissues were placed in 0.5%  
532 uranyl acetate in 30% ethanol before going through a series of 10 minute ethanol washes in  
533 increasing concentration (30-80%) and left for 30 minutes in 100% ethanol. Graded hard  
534 embedding resin 182 (TAAB) was mixed in a 1:1 ratio with 100% ethanol and left on tissues  
535 overnight, then replaced with fresh 100% resin for 30 minutes and placed in an oven at 60°C  
536 for 48 hours to cure. Ultrathin orthogonal serial sections (70-74 nm) were cut through regions  
537 of interest and collected on freshly prepared Pioloform®-coated 200 (for midguts and  
538 proventriculi) or 100 (for proventriculi) mesh nickel grids, before post-staining in uranyl acetate  
539 (5% w/v in 30% ethanol) and 50% lead citrate. Sections were viewed at 100 KV in a FEI Tecnai  
540 G2 Spirit and all micrographs were taken using either an Olympus Megaview3 or a Gatan  
541 Orios camera with AnalySIS or Gatan GMS2 software respectively.

542

### 543 **SBF-SEM and 3D reconstructions**

544 Tissues were prepared and stained for SBF-SEM and 3D reconstruction using a modified  
545 method based on the protocol of Deerinck et al 2010 [58]. Briefly, tsetse midguts were  
546 dissected in ice-cold fixative (0.1M cacodylate, 2% paraformaldehyde (PFA), 2%  
547 glutaraldehyde, 3% sucrose, 2mM calcium chloride pH 7.4) or modified fixative (0.1M  
548 cacodylate, 2% PFA, 2% GA, 3% sucrose, 0.1% tannic acid pH 7.4) followed by washes in  
549 0.1M cacodylate buffer pH 7.4 with 2mM calcium chloride prior to staining with reduced  
550 osmium tetroxide (2%) containing 1.5% potassium ferrocyanide in 0.1M cacodylate buffer.  
551 Midguts were washed in distilled water and incubated in 1% thiocarbohydrazide (TCH) for 30  
552 minutes before further washes in distilled water. A second osmium (2%) staining was carried

553 out at room temperature for 40 minutes, followed by washing in distilled water before  
554 incubation in 1% aqueous uranyl acetate overnight at 4°C. A final wash in distilled water was  
555 carried out and samples were stained in warmed lead aspartate for 30 minutes before  
556 dehydration in graded ethanol 30-90% followed by 100% ethanol. For samples dissected in  
557 modified fixative an additional step was added and samples were placed in 100% propylene  
558 oxide following the series of ethanol washes. Samples were placed in hard resin 812 (TAAB)  
559 at a 1:1 ratio with 100% propylene oxide and left overnight before infiltration with increasing  
560 ratios of resin:propylene oxide until 100% resin and left to cure for 48 hours. Samples were  
561 prepared for SBF-SEM by mounting a small square of embedded sample onto a cryo pin with  
562 conductive epoxy. Excess resin was trimmed away with an ultra-microtome and the sample  
563 coated with 10nm AuPd using a Q150T sputter coater (Quorum Technologies). Samples were  
564 imaged with a FEI Quanta 250 FEG modified with a Gatan 3View running GMS2 software. All  
565 samples were imaged in Low vacuum mode with a chamber pressure of 50 Pa. For the midgut  
566 imaging conditions were 2.2 KV, dwell time of 12  $\mu$ s per pixel, magnification 26 K, giving a  
567 resolution of 3.3 nm in X and Y 100nm in Z over 474 slices of which the first 200 were taken  
568 for reconstruction. For proventriculus imaging conditions were 2 KV, dwell time 12  $\mu$ s per pixel,  
569 magnification 8.7 K and Z was reduced to 40nm and 3 regions of interest (ROI) were scanned,  
570 all of which were 458 with a resolution of 18.7 nm in X and Y. The reconstruction was carried  
571 out on the first 400 slices of ROI 2. GMS2 was used for alignments and conversions to TIFFs  
572 and the reconstructions were carried out using Bitplane Imaris version 8.1.

573

## 574 **Confocal Laser Scanning Microscopy**

### 575 **Whole tissues**

576 *G. m. morsitans* teneral flies (0-24 hours old) were infected with FBS containing 10% rat blood  
577 spiked with either cBSF or BSF AnTat or J10 eGFP BSF trypanosomes (final density of 2 x  
578 10<sup>6</sup> cells) and 10 $\mu$ g/mL wheat germ agglutinin (WGA)-rhodamine. A naïve group (uninfected)  
579 was fed with serum meal only. Flies were fed every day with FBS 10 $\mu$ g/mL WGA-rhodamine

580 and dissected in PBS to score trypanosome infection in midgut and proventriculus. The  
581 proventriculi were fixed in fresh 1% PFA on ice for 1 hour, stained with SiR-actin (1:1000  
582 dilution in PBS, Cytoskeleton Inc.) for 4 hours, incubated with 300ng/mL DAPI for 10 minutes  
583 and mounted in 1% low melting agarose with SlowFade Diamond antifade (ThermoFisher).  
584 Samples were imaged using a Zeiss LSM800 confocal laser scanning microscope.

585

### 586 **Isolated PM**

587 Flies infected with J10 eGFP BSF trypanosomes, were dissected at 5, 9 or 11 dpi and their  
588 peritrophic matrix was dissected out in ice-cold fresh 1% PFA and transferred to poly-lysine  
589 slides for 1 hour. Samples were incubated with 10 $\mu$ g/mL WGA-rhodamine and 300ng/mL  
590 DAPI for 15 minutes, washed and mounted in SlowFade Diamond antifade (ThermoFisher).  
591 Samples were imaged using a Zeiss LSM800 confocal laser scanning microscope.

592

### 593 **Procyclin immunostaining**

594 Teneral flies were infected with BSFs J10 eGFP strain and after 3, 5 or 7 dpi both proventriculi  
595 and midguts were dissected on a glass slide in fresh PBS and each tissue manually ruptured.  
596 Released parasites were harvested and pooled for each tissue and timepoint. Cells were  
597 gently pelleted and fixed in 4% PFA for 30 minutes, before washing in PBS and added to poly-  
598 lysine slides. Cells were left to adhere for 30 minutes at room temperature in a humid chamber  
599 before an hour block in 20% foetal bovine serum in PBS. The following anti-procyclin  
600 antibodies were then added for 1 hour in blocking solution; mAb 9G4 (mouse anti-GPEET  
601 unphosphorylated form, Biorad) 1:200 dilution, mAb 5H3 from hybridoma supernatant (mouse  
602 anti-GPEET phosphorylated form, Professor Terry Pearson) 1:10 dilution and mAb Clone  
603 TBRP1/247 (mouse anti-EP, Cedarlane) 1:800 dilution. The secondary antibody, anti-mouse  
604 IgG conjugated to Alexa Fluor 555 (ThermoFisher) was used at a 1:1000 dilution in blocking  
605 solution for an hour followed by 300 ng/mL of DAPI (ThermoFidsher) for 10 minutes. Samples  
606 were mounted in SlowFade Diamond antifade (ThermoFisher) and imaged using a Zeiss

607 LSM800 confocal laser scanning microscope. Cultured AnTat 1.1 90:13 PCFs were used as  
608 antibody positive controls.

609

### 610 **PM thickness measurements**

611 100 different images from different flies and separate experiments for each time point and  
612 group was used: 5 dpi, 5-day naïve, 11 dpi and 11-day naïve. Each image from each time  
613 point/group was overlaid by a 10x10 square grid and a random number generator (numbers  
614 between 1-10 only) used to determine X and Y squares in which to take measurements.  
615 Measurements were made using ImageJ [59].

616

### 617 **Acknowledgements**

618 We thank Professor Terry Pearson (University of Victoria, Canada) for providing us with anti-  
619 GPEET mouse hybridomas, Dr Lúcia Güther and Professor Mike Ferguson (University of  
620 Dundee) for the generous supply of *T. brucei* sVSG MiTat1.4 variant, Professor Sue Vaughan  
621 (Oxford Brookes University) for making available essential TEM protocols, and Prof Wendy  
622 Gibson for kindly supplying the *T. brucei* J10 strain. We thank Dr Lee Haines for critical reading  
623 of the manuscript, Dr Laura Jeacock for artwork and members of the Acosta Serrano group  
624 for constructive discussions. This work was supported by Wellcome Trust project grant  
625 093691/Z/10/Z (awarded to AAS), Multi-User Equipment Grant (for confocal images  
626 104936/Z/14/Z), GlycoPar-EU FP7 Marie Curie Initial Training Network (GA. 608295)  
627 (awarded to ACS and AAS), MRC Concept in Confidence Award MC\_PC\_17167 (awarded to  
628 AAS) and a PhD studentship from LSTM (awarded to CR).

629

### 630 **Competing interests**

631 The authors declare no conflict of interest.

632

### 633 **Author contributions**

634 CR, NAD, ACS, MJL, and AAS conceived and designed experiments. CR, NAD, AJB, BM,  
635 CS, MJL and IAP conducted and analysed EM work. ACS, CR, NAD and MM obtained  
636 confocal data. CR and AAS wrote the paper with input from all authors.

637

#### 638 **Author ORCIDs**

639 Clair Rose, 0000-0001-7782-5359

640 Aitor Casas-Sánchez, 0000-0001-5237-1223

641 Carla Solórzano, 0000-0001-9129-5569

642 Marco Marcello, 0000-0002-2392-8640

643 Ian Prior, 0000-0002-4055-5161

644 Alvaro Acosta-Serrano, 0000-0002-2576-7959

645

#### 646 **References**

- 647 1. Matthews, K.R., *The developmental cell biology of Trypanosoma brucei*. J Cell Sci, 2005.  
648 **118**(Pt 2): p. 283-90.
- 649 2. Acosta-Serrano, A., et al., *The surface coat of procyclic Trypanosoma brucei: programmed*  
650 *expression and proteolytic cleavage of procyclin in the tsetse fly*. Proc Natl Acad Sci U S A,  
651 2001. **98**(4): p. 1513-8.
- 652 3. Vassella, E., et al., *A major surface glycoprotein of trypanosoma brucei is expressed*  
653 *transiently during development and can be regulated post-transcriptionally by glycerol or*  
654 *hypoxia*. Genes Dev, 2000. **14**(5): p. 615-26.
- 655 4. Van Den Abbeele, J., et al., *Trypanosoma brucei spp. development in the tsetse fly:*  
656 *characterization of the post-mesocyclic stages in the foregut and proboscis*. Parasitology,  
657 1999. **118**(5): p. 469-478.
- 658 5. Vickerman, K., et al., *Biology of African trypanosomes in the tsetse fly*. Biol Cell, 1988. **64**(2):  
659 p. 109-19.
- 660 6. Kleine, *Weitere wissenschaftliche Beobachtungen über die Entwicklung von Trypanosomen in*  
661 *Glossinen1)*. Dtsch med Wochenschr, 1909. **35**(21): p. 924-925.
- 662 7. Lehane, M.J., *Peritrophic matrix structure and function*. Annual Review of Entomology, 1997.  
663 **42**: p. 525-550.
- 664 8. Harmsen, R., *The nature of the establishment barrier for Trypanosoma brucei in the gut of*  
665 *Glossina pallidipes*. Transactions of The Royal Society of Tropical Medicine and Hygiene,  
666 1973. **67**(3): p. 364-373.
- 667 9. Willett, K.C., *Development of Peritrophic Membrane in Glossina (Tsetse Flies) and Its Relation*  
668 *to Infection with Trypanosomes*. Experimental Parasitology, 1966. **18**(2): p. 290-&.
- 669 10. Lehane, M.J. and A.R. Msangi, *Lectin and peritrophic membrane development in the gut of*  
670 *Glossina m.morsitans and a discussion of their role in protecting the fly against trypanosome*  
671 *infection*. Med Vet Entomol, 1991. **5**(4): p. 495-501.
- 672 11. Hao, Z., I. Kasumba, and S. Aksoy, *Proventriculus (cardia) plays a crucial role in immunity in*  
673 *tsetse fly (Diptera: Glossinidae)*. Insect Biochemistry and Molecular Biology, 2003. **33**(11): p.  
674 1155-1164.
- 675 12. Billingsley, P.F. and M.J. Lehane, *Structure and ultrastructure of the insect midgut*, in *Biology*  
676 *of the Insect Midgut*, M.J. Lehane and P.F. Billingsley, Editors. 1996, Springer Netherlands:  
677 Dordrecht. p. 3-30.
- 678 13. Lehane, M.J., P.G. Allingham, and P. Weglicki, *Composition of the peritrophic matrix of the*  
679 *tsetse fly, Glossina morsitans morsitans*. Cell Tissue Res, 1996. **283**(3): p. 375-84.

- 680 14. Rose, C., et al., *An investigation into the protein composition of the teneral Glossina*  
681 *morsitans morsitans peritrophic matrix*. PLoS Negl Trop Dis, 2014. **8**(4): p. e2691.
- 682 15. Rogerson, E., et al., *Variations in the Peritrophic Matrix Composition of Heparan Sulphate*  
683 *from the Tsetse Fly, Glossina morsitans morsitans*. Pathogens (Basel, Switzerland), 2018.  
684 **7**(1): p. 32.
- 685 16. Taylor, A.W., *The Development of West African Strains of Trypanosoma gambiense in*  
686 *Glossina tachinoides under Normal Laboratory*. Parasitology, 1932. **24**(401): p. 401-409.
- 687 17. Yorke, W., F. Murgatroyd, and F. Hawking, *The Relation of Polymorphic Trypanosomes,*  
688 *Developing in the Gut of Glossina, to the Peritrophic Membrane*. Annals of Tropical Medicine  
689 & Parasitology, 2016. **27**(2): p. 347-354.
- 690 18. Freeman, J.C., *The presence of trypanosomes in the ecto-peritrophic space of tsetse flies, half*  
691 *an hour after ingestion of the infective blood meal*. Trans R Soc Trop Med Hyg, 1970. **64**(1):  
692 p. 187-8.
- 693 19. Freeman, J.C., *The penetration of the peritrophic membrane of the tsetse flies by*  
694 *trypanosomes*. Acta Trop, 1973. **30**(4): p. 347-55.
- 695 20. Fairbairn, H., *The penetration of Trypanosoma rhodesiense through the peritrophic*  
696 *membrane of Glossina palpalis*. Ann Trop Med Parasitol, 1958. **52**(1): p. 18-9.
- 697 21. Moloo, S.K., R.F. Steiger, and H. Hecker, *Ultrastructure of the peritrophic membrane*  
698 *formation in Glossina Wiedemann*. Acta Trop, 1970. **27**(4): p. 378-83.
- 699 22. Ellis, D.S. and D.A. Evans, *Passage of Trypanosoma brucei rhodesiense through the*  
700 *peritrophic membrane of Glossina morsitans morsitans*. Nature, 1977. **267**(5614): p. 834-5.
- 701 23. Evans, D.A. and D.S. Ellis, *Recent observations on the behaviour of certain trypanosomes*  
702 *within their insect hosts*. Adv Parasitol, 1983. **22**: p. 1-42.
- 703 24. Evans, D.A. and D.S. Ellis, *The penetrative ability of sleeping-sickness trypanosomes*. Trans R  
704 Soc Trop Med Hyg, 1978. **72**(6): p. 653-5.
- 705 25. Gibson, W. and M. Bailey, *The development of Trypanosoma brucei within the tsetse fly*  
706 *midgut observed using green fluorescent trypanosomes*. Kinetoplastid Biol Dis, 2003. **2**(1): p.  
707 1.
- 708 26. Rogers, M.E., et al., *Leishmania chitinase facilitates colonization of sand fly vectors and*  
709 *enhances transmission to mice*. Cell Microbiol, 2008. **10**(6): p. 1363-72.
- 710 27. Langer, R.C. and J.M. Vinetz, *Plasmodium ookinete-secreted chitinase and parasite*  
711 *penetration of the mosquito peritrophic matrix*. Trends Parasitol, 2001. **17**(6): p. 269-72.
- 712 28. Berriman, M., et al., *The genome of the African trypanosome Trypanosoma brucei*. Science,  
713 2005. **309**(5733): p. 416-22.
- 714 29. Aksoy, E., et al., *Mammalian African trypanosome VSG coat enhances tsetse's vector*  
715 *competence*. Proceedings of the National Academy of Sciences, 2016. **113**(25): p. 6961-6966.
- 716 30. Weiss, B.L., et al., *The peritrophic matrix mediates differential infection outcomes in the*  
717 *tsetse fly gut following challenge with commensal, pathogenic, and parasitic microbes*. J  
718 Immunol, 2014. **193**(2): p. 773-82.
- 719 31. Schuster, S., et al., *Developmental adaptations of trypanosome motility to the tsetse fly host*  
720 *environments unravel a multifaceted in vivo microswimmer system*. Elife, 2017. **6**.
- 721 32. Robertson, M., V. *Notes on the life-history of Trypanosoma gambiense, with a brief reference*  
722 *to the cycles of Trypanosoma nanum and Trypanosoma pecorum in Glossina palpalis*.  
723 Philosophical Transactions of the Royal Society of London. Series B, Containing Papers of a  
724 Biological Character, 1913. **203**(294-302): p. 161-184.
- 725 33. Sharma, R., et al., *Asymmetric cell division as a route to reduction in cell length and change in*  
726 *cell morphology in trypanosomes*. Protist, 2008. **159**(1): p. 137-51.
- 727 34. Butikofer, P., et al., *Phosphorylation of a major GPI-anchored surface protein of*  
728 *Trypanosoma brucei during transport to the plasma membrane*. J Cell Sci, 1999. **112** ( Pt 11):  
729 p. 1785-95.

- 730 35. Tetley, L., et al., *Onset of expression of the variant surface glycoproteins of Trypanosoma*  
731 *brucei in the tsetse fly studied using immunoelectron microscopy*. J Cell Sci, 1987. **87 ( Pt 2)**:  
732 p. 363-72.
- 733 36. Vickerman, K., *On the surface coat and flagellar adhesion in trypanosomes*. J Cell Sci, 1969.  
734 **5(1)**: p. 163-93.
- 735 37. Szempruch, A.J., et al., *Extracellular Vesicles from Trypanosoma brucei Mediate Virulence*  
736 *Factor Transfer and Cause Host Anemia*. Cell, 2016. **164(1-2)**: p. 246-257.
- 737 38. Roditi, I., et al., *Procyclin gene expression and loss of the variant surface glycoprotein during*  
738 *differentiation of Trypanosoma brucei*. J Cell Biol, 1989. **108(2)**: p. 737-46.
- 739 39. Guther, M.L., et al., *GPI-anchored proteins and free GPI glycolipids of procyclic form*  
740 *Trypanosoma brucei are nonessential for growth, are required for colonization of the tsetse*  
741 *fly, and are not the only components of the surface coat*. Mol Biol Cell, 2006. **17(12)**: p. 5265-  
742 74.
- 743 40. Merzendorfer, H., M. Kelkenberg, and S. Muthukrishnan, *Peritrophic Matrices*. 2016. 255-  
744 324.
- 745 41. Vigneron, A., et al., *A fine-tuned vector-parasite dialogue in tsetse's cardia determines*  
746 *peritrophic matrix integrity and trypanosome transmission success*. PLoS Pathog, 2018. **14(4)**:  
747 p. e1006972.
- 748 42. Ridgley, E.L., Z.H. Xiong, and L. Ruben, *Reactive oxygen species activate a Ca<sup>2+</sup>-dependent*  
749 *cell death pathway in the unicellular organism Trypanosoma brucei brucei*. Biochem J, 1999.  
750 **340 ( Pt 1)**: p. 33-40.
- 751 43. Ooi, C.-P., et al., *Tsetse GmmSRPN10 Has Anti-complement Activity and Is Important for*  
752 *Successful Establishment of Trypanosome Infections in the Fly Midgut*. PLOS Neglected  
753 Tropical Diseases, 2015. **9(1)**: p. e3448.
- 754 44. Peters, W., *Peritrophic membranes*. 1992, Berlin ; London: Springer-Verlag. xi, 238 p.
- 755 45. Toh, H., et al., *Massive genome erosion and functional adaptations provide insights into the*  
756 *symbiotic lifestyle of Sodalis glossinidius in the tsetse host*. Genome Res, 2006. **16(2)**: p. 149-  
757 56.
- 758 46. Escott, G.M. and D.J. Adams, *Chitinase activity in human serum and leukocytes*. Infect  
759 Immun, 1995. **63(12)**: p. 4770-3.
- 760 47. Beschin, A., et al., *African trypanosome control in the insect vector and mammalian host*.  
761 Trends in Parasitology, 2014. **30(11)**: p. 538-547.
- 762 48. Oberholzer, M., et al., *Social motility in African trypanosomes*. PLoS Pathog, 2010. **6(1)**: p.  
763 e1000739.
- 764 49. Imhof, S., et al., *A Glycosylation Mutant of Trypanosoma brucei Links Social Motility Defects*  
765 *In Vitro to Impaired Colonization of Tsetse Flies In Vivo*. Eukaryotic cell, 2015. **14(6)**: p. 588-  
766 592.
- 767 50. Lopez, M.A., E.A. Saada, and K.L. Hill, *Insect stage-specific adenylate cyclases regulate social*  
768 *motility in African trypanosomes*. Eukaryot Cell, 2015. **14(1)**: p. 104-12.
- 769 51. Imhof, S., et al., *Social motility of African trypanosomes is a property of a distinct life-cycle*  
770 *stage that occurs early in tsetse fly transmission*. PLoS Pathog, 2014. **10(10)**: p. e1004493.
- 771 52. Imhof, S. and I. Roditi, *The Social Life of African Trypanosomes*. Trends Parasitol, 2015.  
772 **31(10)**: p. 490-498.
- 773 53. Bastin, P. and B. Rotureau, *Social motility in African trypanosomes: fact or model?* Trends  
774 Parasitol, 2015. **31(2)**: p. 37-8.
- 775 54. Mehrlitz, D., et al., *Epidemiological studies on the animal reservoir of Gambiense sleeping*  
776 *sickness. Part III. Characterization of trypanozoon stocks by isoenzymes and sensitivity to*  
777 *human serum*. Tropenmed Parasitol, 1982. **33(2)**: p. 113-8.
- 778 55. Bingle, L.E., et al., *A novel GFP approach for the analysis of genetic exchange in*  
779 *trypanosomes allowing the in situ detection of mating events*. Microbiology, 2001. **147(Pt**  
780 **12)**: p. 3231-40.

- 781 56. Ziegelbauer, K., et al., *Synchronous differentiation of Trypanosoma brucei from bloodstream*  
782 *to procyclic forms in vitro*. Eur J Biochem, 1990. **192**(2): p. 373-8.
- 783 57. MacGregor, P., et al., *Stable transformation of pleomorphic bloodstream form Trypanosoma*  
784 *brucei*. Molecular and biochemical parasitology, 2013. **190**(2): p. 60-62.
- 785 58. Deerinck, T.J., et al., *NCMIR methods for 3D EM: a new protocol for preparation of biological*  
786 *specimens for serial block face scanning electron microscopy*. Microscopy, 2010: p. 6-8.
- 787 59. Schneider, C.A., W.S. Rasband, and K.W. Eliceiri, *NIH Image to ImageJ: 25 years of image*  
788 *analysis*. Nature Methods, 2012. **9**: p. 671.
- 789
- 790